




ARTICLE

DOI: 10.1038/s41467-018-03235-7

OPEN

Single rhodium atoms anchored in micropores for efficient transformation of methane under mild conditions

Yu Tang ¹, Yuting Li¹, Victor Fung², De-en Jiang ², Weixin Huang^{1,3}, Shiran Zhang^{1,3}, Yasuhiro Iwasawa⁴, Tomohiro Sakata⁴, Luan Nguyen^{1,3}, Xiaoyan Zhang^{1,5}, Anatoly I. Frenkel^{6,7} & Franklin (Feng) Tao ^{1,3}

Catalytic transformation of CH₄ under a mild condition is significant for efficient utilization of shale gas under the circumstance of switching raw materials of chemical industries to shale gas. Here, we report the transformation of CH₄ to acetic acid and methanol through coupling of CH₄, CO and O₂ on single-site Rh₁O₅ anchored in microporous aluminosilicates in solution at ≤150 °C. The activity of these singly dispersed precious metal sites for production of organic oxygenates can reach about 0.10 acetic acid molecules on a Rh₁O₅ site per second at 150 °C with a selectivity of ~70% for production of acetic acid. It is higher than the activity of free Rh cations by >1000 times. Computational studies suggest that the first C–H bond of CH₄ is activated by Rh₁O₅ anchored on the wall of micropores of ZSM-5; the formed CH₃ then couples with CO and OH, to produce acetic acid over a low activation barrier.

¹Department of Chemical and Petroleum Engineering and Department of Chemistry, University of Kansas, Lawrence, KS 66045, USA. ²Department of Chemistry, University of California, Riverside, CA 92521, USA. ³Department of Chemistry and Biochemistry, University of Notre Dame, Notre Dame, IN 46556, USA. ⁴Innovation Research Center for Fuel Cells and Graduate School of Informatics and Engineering, The University of Electro-Communications, Chofu, Tokyo 182-8585, Japan. ⁵State Key Laboratory of Photocatalysis on Energy and Environment and College of Chemistry, Fuzhou University, Fuzhou 350116, China. ⁶Department of Materials Science and Chemical Engineering, Stony Brook University, Stony Brook, NY 11794, USA. ⁷Division of Chemistry, Brookhaven National Laboratory, Upton, NY 11973, USA. Correspondence and requests for materials should be addressed to F.T. (email: franklin.feng.tao@ku.edu)

CH₄ has been one of the inexpensive energy resources since the maturation of hydraulic fracturing technology. So far, most processes of transformation of CH₄ to intermediate compounds for chemical industries including steam or dry reforming, partial oxidation, and oxidative coupling are performed at high temperatures. One side effect of these processes is the deactivation of catalysts due to coke formation^{1,2}. Another is the input of huge amount of energy since they are performed at high temperatures. Thus, activation of C–H of CH₄ at a low temperature is necessary in order to transform shale gas to intermediate compounds of chemical industries in an energy-efficient manner^{3–9}.

Acetic acid is one of the important intermediates of chemical industries. The global demand is 6.5 million metric tons per year (Mt/a). Currently, it is produced from methanol carbonylation, in which CO reacts with methanol to form acetic acid. However, methanol is synthesized from CO and H₂, which are produced from steam reforming processes of either methane or coal at high temperatures¹⁰. Replacement of the current high-temperature catalysis toward production of acetic acid with catalysis at low temperatures would be feasible if a catalytic process on a heterogeneous catalyst could efficiently, directly transform CH₄ to acetic acid under a mild condition. Transformations of methane to methanol and acetic acid on isolated palladium and rhodium atoms anchored in zeolite in liquid solution were simultaneously explored in our group since early 2012. We reported oxidation of methane to form methanol on Pd₁O₄ anchored in ZSM-5 in aqueous solution at low temperature in 2016¹¹. Other than the mild oxidation of CH₄ to CH₃OH with supported isolated Pd atoms anchored in ZSM-5, we have simultaneously studied oxidation of methane through coupling with CO and O₂ to methanol and acetic acid on isolated Rh atom anchored in ZSM-5 since 2012 and the Rh₁O₅/ZSM-5 catalyst was synthesized and its high activity was confirmed and its structure was identified before summer of 2014.

Formation of single sites is a significant approach to developing catalyst toward high catalytic activity and selectivity^{11–17}. Separately anchoring catalytic sites (M₁) on an oxide support (M₁/A_xO_y) tunes the electronic state of catalytic sites of metal atoms (M₁), which are typically continuously packed on surface of a metal nanoparticle or periodically located in a surface lattice of a metal oxide nanoparticle (M_xO_y). Compared to continuously packed M atoms on surface of a metal nanoparticle (···M–M–M···) and periodically packed M cations in surface lattice of a metal oxide nanoparticle (···O–M₁–O–M₁⁺–O–M₁–O–M₁–O···), these isolated cation sites (M₁⁺) anchored on surface of a substrate oxide (A_xO_y), ···O–A–O–M₁⁺–O–A–O–A, exhibit a distinctly different coordination of M atoms. Thus, those isolated cations (M₁) could exhibit a catalytic performance distinctly different from a metal oxide nanoparticle (M_xO_y) or a metal nanoparticle.

We separately anchored Rh cations on the internal surface of micropores of an aluminosilicate, H-ZSM-5 through ion exchange between Rh³⁺ in solution and H⁺ on the internal surface of micropore, similar to the isolated palladium atoms in ZSM-5¹¹. As these Bronsted sites are typically isolated, Rh³⁺ cations can be separately anchored on Bronsted sites. Production of acetic acid through coupling CH₄ with CO and O₂ (2CH₄+2CO+O₂→2CH₃COOH) is efficiently catalyzed by these singly dispersed Rh sites, Rh₁O₅. Different from rhodium atoms anchored on nonporous silicate and other nonporous oxide, this heterogeneous catalyst exhibits high activity in transforming CH₄ to acetic acid, about 0.1 CH₃COOH molecules per Rh site per second with a selectivity of ~70% for production of acetic acid. Isotope-labeled experiments using ¹³CH₄ and ¹³CO show that CH₃ of CH₃COOH forms from activation of CH₄ to CH₃ and C=O of CH₃COOH from insertion CO to Rh–OH. Density

functional theory (DFT) calculation suggests that activation of C–H of CH₄ and O–O of O₂ are performed on a Rh₁ atom and thus CH₃– and HO are formed on the Rh₁ atom. Insertion of C'O' to Rh₁–O bond of –Rh₁–OH to form a –Rh₁–C'O'OH on Rh₁ atom; the formed –Rh₁–C'O'OH couples with CH₃ adsorbed on the same Rh₁ atom, generating the first product molecule, CH₃C'O'OH. The left –Rh₁=O activates the second CH₄ to form CH₃ and HO; the formed CH₃ couples with CO to form acetyl, which couples with adsorbed HO to form the second acetic acid molecule.

Results

Preparation of isolated Rh catalytic site in ZSM-5. Rh cations were introduced to the internal surface of micropores of ZSM-5 through a method integrating vacuum pumping and incipient wetness impregnation (IWI). To minimize the amount of Rh cations to be deposited on external surface of a ZSM-5 particle, solution of Rh³⁺ with the same volume as the pore volume of ZSM-5 was slowly dropped to ZSM-5 powder with a syringe pump when the catalyst powder was continuously stirred and remained in vacuum. During IWI, Rh cations exchanged with singly dispersed Brønsted acid sites of H-ZSM-5, which was prepared through calcining NH₄-ZSM-5 at 400 °C for 12 h. After the introduction of Rh³⁺, the samples were further dried in an oven at 80 °C for 3 h and calcined in air at 550 °C for 3 h, forming the catalyst, Rh/ZSM-5. The evolution of the chemical environment of Rh cations in ZSM-5 was shown in Supplementary Fig. 1. The concentration of Rh cations in the as-synthesized catalyst was measured through inductively coupled plasma atomic emission spectroscopy (ICP-AES). Before an ICP-AES measurement, 28 mg of 0.10 wt%Rh/ZSM-5 was dissolved in aqua regia. For catalyst with a nominal mass ratio of Rh to aluminosilicate, 0.10 wt%, the measured weight percent was 0.10 wt%, which suggests no obvious loss of Rh atoms during the preparation. X-ray photoelectron spectroscopy (XPS) studies of the as-synthesized 0.10 wt%Rh/ZSM-5 show the lack of Rh atoms in surface region of catalyst particles (red spectrum in Fig. 1c). The lack of Rh atoms in surface region revealed with XPS together with the 0.10 wt%Rh in the as-synthesized catalyst measured with ICP-AES suggests that these introduced Rh atoms were anchored in micropores of ZSM-5 particles instead of the external surface of ZSM-5 particles. At a high loading (0.50 wt%Rh/ZSM-5), unfortunately rhodium oxide nanoparticles (2–4 nm) were formed as evidenced by the low contrast patches in transmission electron microscopy (TEM) image (Fig. 1b), consistent with the observed Rh 3d photoemission feature in studies of sample using XPS (black spectrum in Fig. 1c)¹⁸.

The existence of Rh atoms in the micropores of ZSM-5 after catalysis was confirmed by the measured concentration of Rh atoms remained in micropores with ICP-AES, which was 0.098%. Extended X-ray absorption fine structure spectroscopy (EXAFS) was used to characterize the chemical environment of anchored Rh atoms of used 0.10 wt%Rh/ZSM-5 (the catalyst after reaction). After catalysis, the used catalyst powder was centrifuged and thus washed with deionized H₂O several times and then dried in oven at 200 °C. The obtained powder was used for EXAFS studies in flowing He at 150 °C. r-space spectrum of K-edge of Rh atoms of the used catalyst show that Rh atoms bond with oxygen atoms and the average coordination number of oxygen atoms to a Rh atom is CN(Rh–O) of 5.23 ± 0.52 (Fig. 1e, f). Notably, no contribution of Rh–Rh metal bonds was needed to fit the r-space spectrum of Rh K-edge (Fig. 1e), suggesting that there is no evidence for formation of Rh–Rh metal bonds. This is consistent with the oxidation state of Rh shown in Fig. 1h. Similar to literature^{19–21}, the second shell of rhodium oxide at 2.60 Å in r-

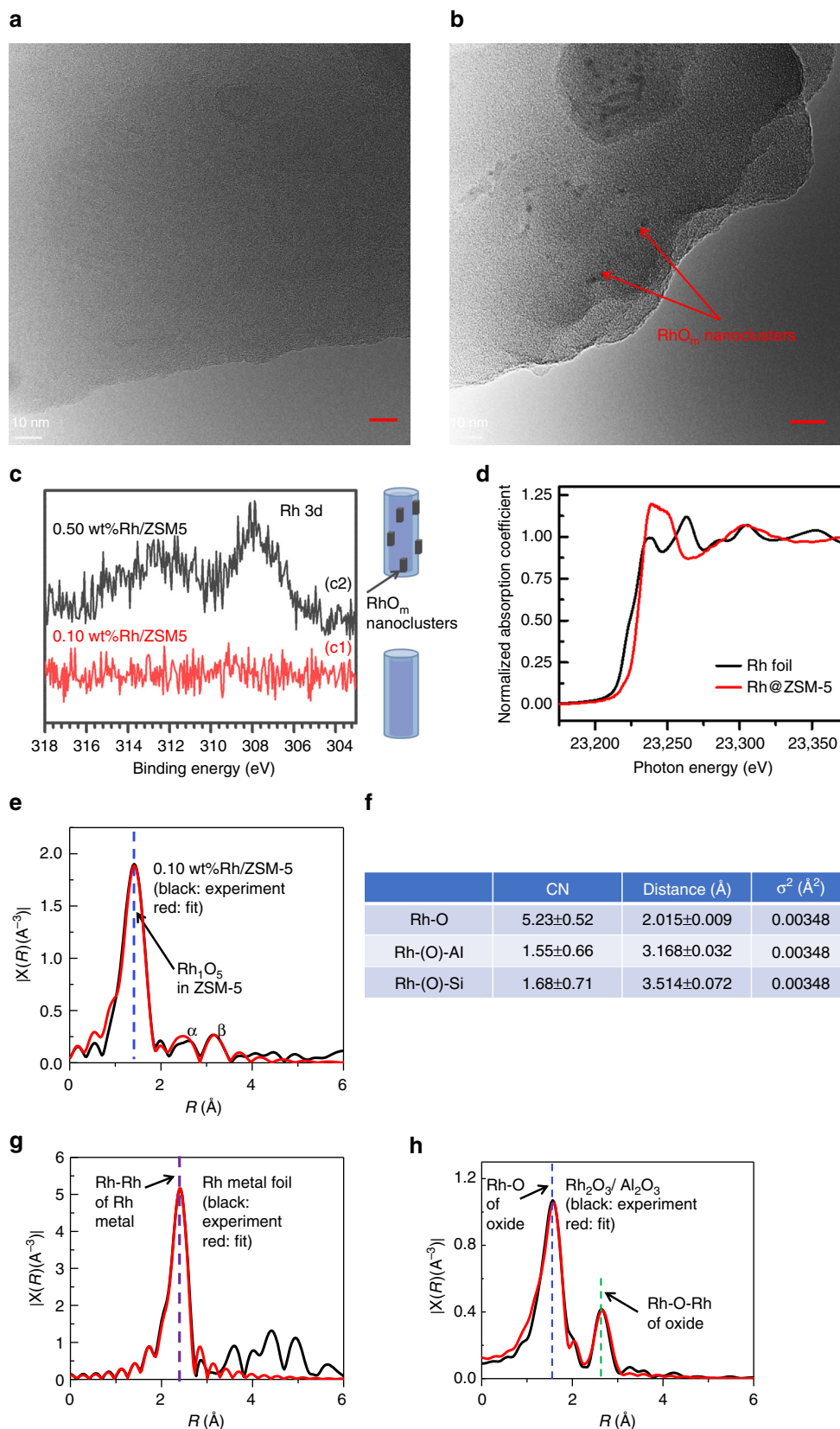


Fig. 1 Structural characterization of isolated rhodium atoms in ZSM-5. **a** TEM image of particles of 0.10 wt%Rh/ZSM-5; scale bar: 10 nm. **b** TEM image of particles of 0.50 wt%Rh/ZSM-5; scale bar: 10 nm. **c** Rh 3d XPS peak of 0.10 wt%Rh/ZSM-5 and 0.50 wt%Rh/ZSM-5. **d** Energy space of Rh K-edge of 0.10 wt%Rh/ZSM-5 and Rh foil (reference sample) of X-ray absorption near edge spectra (XANES). **e** r-space of Rh K-edge of experimental (black) and calculated (red) data of the k^2 -weighted Rh K-edge EXAFS spectra of used 0.10 wt%Rh/ZSM-5. **f** Coordination number and bond length on average of the used 0.10 wt%Rh/ZSM-5. **g** r-space of Rh K-edge of experimental (black) and calculated (red) data of the k^2 -weighted Rh K-edge EXAFS spectra of Rh metal foil. **h** r-space of Rh K-edge of experimental (black) and calculated (red) data of the k^2 -weighted Rh K-edge EXAFS spectra of Rh₂O₃ nanoparticles supported on Al₂O₃

space spectrum (Fig. 1h) was clearly observed in our reference sample Rh₂O₃ nanoparticles. However, there is lack of Rh–O–Rh peak at 2.60 Å in the r-space spectrum of 0.10 wt%Rh/ZSM-5 (black line in Fig. 1e). It shows Rh atoms of our used catalyst do not have the second coordination shell of Rh atoms in terms of lack of Rh–O–Rh and thus there are no rhodium oxide nanoclusters formed in our used catalyst (0.10 wt%Rh/ZSM-5). Inspired by work of Gates group^{14,22}, particularly the assignment of intensity at about 2.7 Å in r-space spectrum of Rh K-edge to Rh–O–Al with a Rh–(O)–Al distance of 3.02 Å^{14,23–25}, we fit the small peak (α) at about 2.7 Å in Fig. 1e to Rh–O–Al. In addition, we fit the intensity at about 3.3 Å (β) in r-space of Rh K-edge to Rh–O–Si (Fig. 1e); the coordination numbers of Al to Rh through O atom and Si to Rh through O atom are 1.55 ± 0.66 and 1.68 ± 0.71, respectively; the distances of Al and Si atoms to the Rh atoms are 3.168 ± 0.032 Å and 3.514 ± 0.072 Å, respectively. Thus, these EXAFS studies show that Rh atoms of 0.10 wt%Rh/ZSM-5 are singly dispersed in micropores of ZSM-5 and each Rh atom bond with about five oxygen atoms on average. In the following paragraphs, sometimes we used Rh₁O₅@ZSM-5 when we need to point out the coordination environment of the Rh atoms on average. Supplementary Fig. 1f schematically shows the structure of a catalytic site of Rh₁O₅ anchored in micropores of ZSM-5.

The replacement of Brønsted acid sites (BAS) of H-ZSM-5 by Rh cations was confirmed with ¹H NMR (nuclear magnetic resonance) of 0.10 wt%Rh/ZSM-5 and H-ZSM-5. As shown in Supplementary Fig. 2a, the peak at 4.6 ppm was assigned to BAS site of H-ZSM-5 (Supplementary Table 1)^{26,27}. It was not obviously observed in the same region of chemical shift in Supplementary Fig. 2b. This difference in Supplementary Fig. 2 suggests that the loss of some BAS sites due to ion exchange of Rh³⁺ with H⁺ in the IWI process.

Catalytic performance of Rh₁O₅@ZSM-5 at 150 °C. Catalytic activities of pure H-ZSM-5 and as-prepared Rh/ZSM-5 catalysts were measured by adding 28 mg catalyst to 10 mL deionized water in a Parr high-pressure reactor (Supplementary Fig. 3b). The aqueous solution with dispersed catalyst particles was continuously, vigorously stirred by a magnetic bar coated with plastic materials at a speed of 600 rpm during catalysis. A mixture of CH₄, CO, and O₂ with different partial pressure was introduced to the Parr reactor at room temperature. A portion of these reactant gases with a relatively high-pressure can diffuse to micropores of catalyst dispersed in the solvent (H₂O or dodecane) and thus be catalyzed. Then, the reactor was heated to a set temperature. The reaction temperature of the solvent was directly measured through a thermocouple probe submerged to the solution consisting of the dispersed catalyst particles and solvent in the Parr reactor. The preservation of catalysis temperature for certain amount of time were performed by a temperature controller. This chemical transformation was performed for certain amount of time. The pressure, reaction temperature, and reaction time of each measurement of catalytic performance were given in the following figures and tables. Catalytic reaction under each condition was repeated at least four times.

After each catalytic reaction, the solution in the Parr reactor consisting the used catalyst powder and liquid products was filtrated to separate the used catalyst powder. The clear liquid obtained after filtering the catalyst powder mainly contains acetic acid, methanol, formic acid, and solvent. The product solution was analyzed by ¹H NMR and ¹³C NMR. The measurement was calibrated with 3-(trimethylsilyl)-1-propanesulfonic acid sodium salt (DSS) with chemical shift at δ = 0.0 ppm^{11,28}. A DSS solution was prepared by dissolving DSS to D₂O, making a solution with concentration of DSS in D₂O at 0.020 wt%. Typically, 0.70 mL of

the obtained clear liquid solution was mixed with 0.10 mL of as-prepared DSS solution in an NMR tube before NMR analysis. The identified oxygenate products were acetic acid (δ = 2.08 ppm), formic acid (δ = 8.28 ppm) and methanol (δ = 3.33 ppm). A solvent suppression program was applied for minimizing the signal originating from H₂O, similar to our previous studies^{11,28}. Supplementary Fig. 4 is a representative NMR spectrum of solution after catalysis; peak of DSS was marked on it. To quantify the amounts of products, standard curves of acetic acid, formic acid, and methanol were carefully established and shown in Supplementary Fig. 5. The analysis was described in the Methods section.

With 28 mg of 0.10 wt%Rh/ZSM-5, 226.1 μmol of total products (acetic acid, formic acid, and methanol) were produced at 150 °C in the first hour (entry 4 in Supplementary Table 2). Under the same condition, unfortunately the yields of the total organic compounds formed from 0.50 wt%Rh/ZSM-5 (entry 5 in Supplementary Table 2) are similar to 0.10 wt%Rh/ZSM-5. The similarity in catalytic performances of the two catalysts shows that the rhodium oxide nanoparticles formed on the surface of 0.50 wt%Rh/ZSM-5 are not active for this transformation. In other words, the catalytic activity of 0.10 wt%Rh/ZSM-5 in the production of acetic acid was contributed from the Rh₁O₅ sites anchored in micropores of ZSM-5 instead of rhodium oxide nanoparticles supported on the external surface of ZSM-5. As the conversions of CH₄ in these studies of Fig. 2 and Table 1 are lower than 20%, we used these conversions and yields to calculate the turn-over rates with the equation:

$$\text{TOR} = \frac{\text{Number of produced molecules}}{\text{Time of catalytic reaction (S)} \times \text{Number of active sites (Rh}_1\text{O}_5)} \quad (1)$$

This calculation is based on an assumption that all loaded Rh atoms are active sites. This calculation was further described in Supplementary Methods. The activities for production of acetic acid and total organic oxygenates including acetic acid, methanol and formic acid at 150 °C are 0.070 and 0.10 molecules per Rh atom per second (entry 2 of Table 1), respectively.

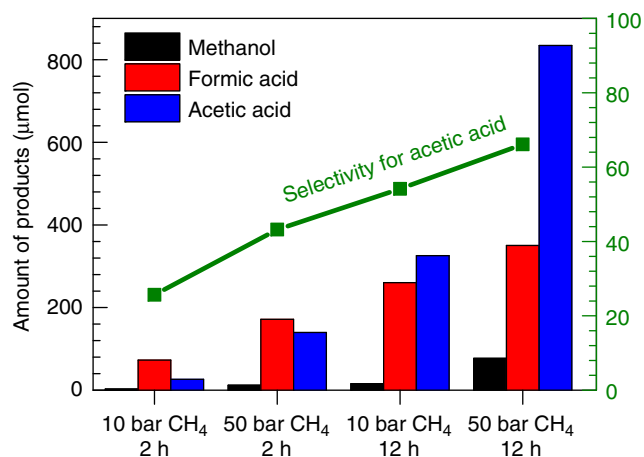


Fig. 2 Catalytic performance of 0.10 wt%Rh/ZSM-5. Yields of acetic acid, formic acid and methanol as well as the selectivity to acetic acid as a function of different pressures of CH₄ (10 or 50 bars) and different reaction times (2 h or 12 h). 28 mg of 0.10 wt%Rh/ZSM-5 was used for each catalysis test. Each catalysis test used 10 bar CO and 8 bar O₂ and certain pressure of CH₄ as noted on x-axis (10 or 50 bars). The catalysis temperatures of all studies here were 150 °C

Table 1 Comparison of TOR for formation of acetic acid or oxygenates including acetic acid, formic acid and methanol on 0.10 wt %Rh/ZSM-5

Entry	Catalyst	Catalytic temperature	TOR of acetic acid (molecule per site per second)	TOR of organic oxygenate ^a (number of molecules per site per second)	Selectivity for production of acetic acid
1	0.10 wt%Rh/ZSM-5 ^a	150 °C	0.040 ^b	0.099 ^b	40.0%
2	0.10 wt%Rh/ZSM-5 ^a	150 °C	0.070 ^c	0.10 ^c	70.1%
3	Rh(NO ₃) ₃ ^a	150 °C	6.3 × 10 ⁻⁶ ^d	2.4 × 10 ⁻⁵ ^d	26.3%

^a Here the organic oxygenates include acetic acid, formic acid and methanol (CO₂ was not included). Calculations of TORs of these catalysts were described in Supplementary Methods

^b The catalysis condition of 0.10 wt%Rh/ZSM-5: mixture of 50 bar CH₄, 10 bar CO, 8 bar O₂, 2 h; the yields of acetic acid and all organic oxygenates were plotted in Fig. 2

^c The catalysis condition of 0.10 wt%Rh/ZSM-5: mixture of 50 bar CH₄, 10 bar CO, 8 bar O₂, 12 h; the yields of acetic acid and all organic oxygenates were listed in Fig. 2

^d Rh(NO₃)₃ was used in literature³². Five milliliters of 0.01 mol/L Rh(NO₃)₃ was added in Parr reactor and 50 bar CH₄, 10 bar CO, and 8 bar O₂ were introduced to the Parr reactor and then the Parr reaction was sealed; the reaction was performed at 150 °C for about 90 h. This measurement was done for comparison with 0.10 wt%Rh/ZSM-5 in which Rh₁ cations were anchored in micropores

Table 2 Catalytic performances of 28 mg catalysts of 0.10 wt%Rh supported on different supports in a mixture of 10 bar CH₄, 10 bar CO, and 8 bar O₂ at 150 °C for 3 h with 10 mL H₂O in a high-pressure reactor

Entry	Samples	Methanol (μ mol)	Formic acid (μ mol)	Acetic acid (μ mol)	Total products (μ mol)
1	H-ZSM-5	3.67	2.28	1.87	7.82
2	0.10%Rh/SiO ₂	8.70	4.62	6.13	19.46
3	0.10%Rh/Al ₂ O ₃	5.68	0.91	3.05	9.64

Acetic acid, formic acid, and methanol were identified as products. Reactants on pure H-ZSM-5 was also performed at the same conditions as blank experiment (entry 1)

To check whether Rh atoms anchored in micropores of ZSM-5 could detach from ZSM-5, the clear solution was obtained by filtration for removal of Rh/ZSM-5 catalyst particles from the solution after catalysis at 150 °C for 12 h. ICP-AES test of this solution shows that only 2% of the total Rh atoms of 28 mg of 0.10 wt%Rh/ZSM-5 detached from ZSM-5 to solution. Thus, most Rh atoms remained in ZSM-5 after catalysis. Due to the negligible amount of Rh³⁺ detached from 0.10 wt%Rh/ZSM-5 and the extremely low TOF of free Rh³⁺ in solution evidenced in entry 3 in Table 1, contribution of the detached Rh³⁺ to the measured catalytic activity in formation of acetic acid is negligible. It suggests that the anchored Rh atoms are the active sites.

To further confirm the contribution of Rh₁O₅ sites to the formation of acetic acid, control experiments were performed on these catalysts including 28 mg of H-ZSM-5, 28 mg of 0.10 wt% Rh/SiO₂ and 28 mg of 0.10 wt%Rh/Al₂O₃ under the exactly same condition as that of 28 mg 0.10 wt%Rh/ZSM-5 at 150 °C in the mixture of 10 bar CH₄, 10 bar CO and 8 bar O₂ for 4 h. As shown in Table 2, the amounts of acetic acid, formic acid, or methanol produced on 28 mg of 0.10 wt%Rh/SiO₂ and 28 mg of 0.10 wt% Rh/Al₂O₃ are lower than 10 μmol, which are at the level of error bar. All the reported yields in this communication are the measured products formed from 28 mg catalyst. The yield could be shown as μmol/gram catalyst by multiplying a factor of $\frac{1000 \text{ mg/gram}}{28 \text{ mg}}$. For example, the measured yields of methanol and acetic acid on 28 mg of 0.10%Rh/SiO₂ are 8.70 and 6.13 μmol, respectively; if they are multiplied by the factor $\frac{1000 \text{ mg/gram}}{28 \text{ mg}}$ they seem to indicate that 310 μmol methanol and 218 μmol acetic acid could form from one gram of 0.10%Rh/SiO₂ catalyst. Here, the multiplication is not meaningful since the values in Table 2 are at the uncertainty level. As the measured 8.70 μmol methanol and 6.13 μmol acetic acid from 28 mg 0.10%Rh/SiO₂ catalyst are in the range of error bar of these measurements, these values are not used to predict activity of 1 gram to compare with other catalysts. Even if the multiplication factor were applied, the activity of 0.10%Rh/SiO₂ is significantly lower than 0.10 wt%Rh/

ZSM-5. For instance, 218 μmol acetic acid from per gram 0.10% Rh/SiO₂ calculated from the measured 6.13 μmol acetic acid per 28 mg is still much lower than 5000 μmol acetic acid from per gram 0.10 wt%Rh/ZSM-5 calculated from the measured 140 μmol acetic acid per 28 mg catalyst. In conclusion, these control samples in terms of Rh supported on these nonporous oxides and even on a couple of commonly used reducible oxides are not active for the production of acetic acid or methanol from coupling of CH₄ with CO and O₂. Thus, these studies suggest the significant contribution of Rh₁O₅ sites encapsulated in ZSM-5 to the formation of acetic acid.

The participation of all these three reactants (CH₄, CO, and O₂) was confirmed with three parallel studies on 0.10 wt%Rh/ZSM-5 under the exactly same catalytic condition as listed in Supplementary Fig. 6a, b, c; in each of these studies, only two of the three reactants were introduced to the Parr reactor; none of these studies produced acetic acid, formic acid, or methanol due to the lack of the third reactant gas. Those studies clearly show that all the three gases (CH₄, CO, and O₂) are necessary reactants for the formation of CH₃COOH. The necessity of the three reactants was supported by DFT calculations described later.

Participation of molecular O₂ in synthesis of acetic acid. Here, we used low-cost molecular oxygen (O₂) or compressed air as oxidant in oxidative transformation of CH₄ and CO to acetic acid. To further confirm the direct participation of molecular O₂, we performed catalysis at different pressures of O₂ (2, 4, 8, 12, and 16 bar) but all other conditions are the same in these parallel studies; in each of these parallel studies, 28 mg of 0.10 wt%Rh/ZSM-5 was added to 10 mL H₂O. The reaction was performed at 150 °C for 2 h in a mixture of 35 bar CH₄, 10 bar CO and different pressures of O₂, in order to investigate the correlation of yields of products (acetic acid, formic acid, and methanol) with pressure of O₂. As shown in Fig. 3a, highest yields of acetic acid and formic acid were obtained from the catalysis using 8 bar O₂. The increase of yield of acetic acid and formic acid along the increase of O₂ pressure shows that O₂ does participate in the formation of acetic

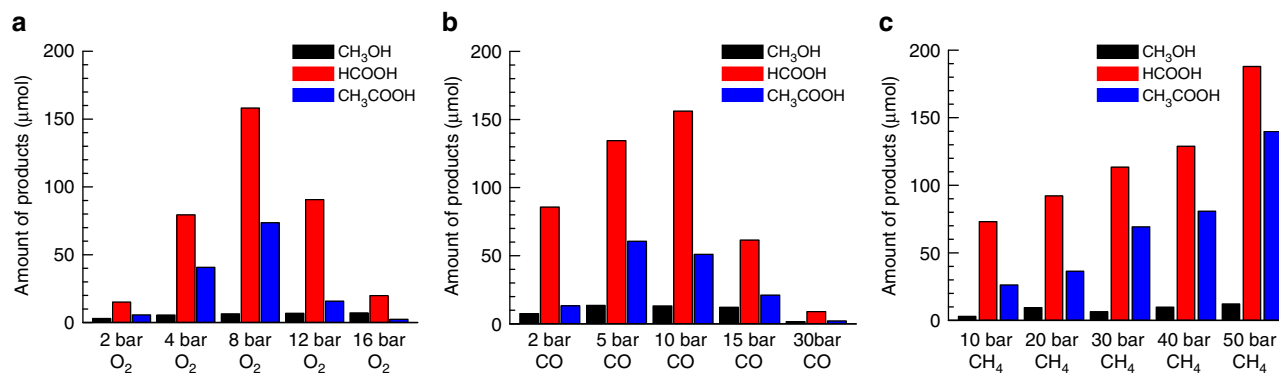


Fig. 3 Influence of partial pressure O₂, CO and CH₄ on catalytic performances. Yields of methanol (black), formic acid (blue), and acetic acid (red) in the chemical transformation of CH₄ at 150 °C in aqueous solutions at different pressure of O₂, CO, CH₄. **a** 35 bar CH₄, 10 bar CO, and different pressure of O₂ at 150 °C for 2 h. **b** 50 bar CH₄, 8 bar O₂, and different pressure of CO at 150 °C for 1.5 h. **c** 10 bar CO, 8 bar O₂ and different pressure of CH₄ at 150 °C for 2 h

acid and formic acid. It is expected that high coverage of oxygen atoms on a Rh atom achieved with high-pressure O₂ could saturate Rh₁ atom with oxygen atoms, which poisons catalytic sites and thus results in a low yield of oxygenates at high pressure of O₂.

Direct participation of CO to synthesis of acetic acid. To further confirm the participation of CO in the formation of acetic acid, influence of the partial pressure of CO on both the conversion of CH₄ and selectivity for production of acetic acid was investigated through parallel studies (Fig. 3b). In each of these studies, the partial pressures of CH₄ and O₂ were fixed at 50 and 8 bar, respectively. However, the pressures of CO in the five studies are 2, 5, 10, 15, and 30 bar. The increase of the amount of acetic acid while CO pressure was increased from 2 to 10 bar suggests that CO directly participates into the formation of acetic acid. However, the lack of activity for production of acetic acid at 30 bar CO showed that catalyst sites were blocked at such a high-pressure of CO. Clearly, CO molecules must have directly interacted with the Rh cations. At high-pressure of CO, high coverage of CO could saturate the coordination of a Rh₁ atom and thus deactivate this catalyst. We measured the concentrations of Rh in the liquid (α) after filtration of the catalyst experienced the catalysis at 10 bar CO, 50 bar CH₄, and 8 bar O₂ for 2.5 h, and in another liquid (β) after filtration of the catalyst experienced the catalysis at 30 bar CO, 50 bar CH₄, and 8 bar O₂. The amounts of Rh atoms in the liquids α and β are 2.0% and 13.0% of all Rh atoms of 28 mg of 0.10 wt%Rh/ZSM-5, respectively. Thus, the much larger loss of Rh atoms at high-pressure of CO (30 bar) suggests that Rh atoms formed carbonyl in CO at high-pressure and some of these formed rhodium carbonyl species desorbed from micropores and then dissolved in the solution. Thus, some Rh species detached at high pressure of CO.

A molecular-level evidence on direct participation of CO in the synthesis of acetic acid is the following isotope experiment. 0.7 bar ¹³CO (Aldrich, 99%, total pressure 2.5 bar) was mixed with 6.3 bar of CO, 14 bar CH₄, and 8 bar O₂ for catalysis of 10 h (Fig. 4a). As the chemical shift of ¹³CH₃OH in ¹³C spectrum can be readily distinguished from acetic acid and formic acid, 40 μmol of ¹³CH₃OH (Aldrich, 99 at%) was added to the collected solution after catalysis as a reference to quantify the amount of potential isotope products ¹³CH₃COOH, CH₃¹³COOH, or H¹³COOH. As the unlabeled CO gas has a natural abundance of ¹³C of 1.10%, a small amount of CH₃¹³COOH or H¹³COOH can form from the natural 1.10% ¹³CO of unlabeled CO gas tank. Contrast experiments using the mixture of 7 bar of CO, 14 bar CH₄, and

8 bar O₂ were performed (Fig. 4b). The intensity ratio of the formed CH₃¹³COOH to ¹³CH₃OH in the solution of isotope experiment using ¹³CO (Fig. 4a) is obviously larger than those formed in the contrast experiment using unlabeled CO (Fig. 4b) by 6.4 times; in addition, the intensity ratio of H¹³COOH to ¹³CH₃OH in isotope experiment (Fig. 4a) is higher than that in the contrast experiment by 2.6 times (Fig. 4b). They suggested that the C' atoms of CH₃C'OOH and HC'OOH came from C'O molecules. Notably, the intensity ratio of ¹³CH₃COOH to reference (¹³CH₃OH) in isotope experiment (Fig. 4a) is the same as the ratio of the contrast experiment (Fig. 4b). It suggests that the C atoms of CH₃ of CH₃COOH do not come from the reactant CO.

One potential pathway to form acetic acid is the coupling of CO with a formed formic acid molecule; if so, yield of acetic acid should increase along the increase of CO pressure. However, as shown in Fig. 3b yield of acetic acid decreases along with the increase of CO pressure (≥10 bar). Thus, coupling formic acid with CO to form acetic acid is not a pathway. To further check the possibility of reaction between HCOOH and CO to form acetic acid, we performed three control experiments at 150 °C for 3 h under the following conditions including mixture of 28 mg 0.10 wt%Rh/ZSM-5, 108 μmol HCOOH, and 10 mL DI H₂O without any CO, mixture of 28 mg 0.10 wt%Rh/ZSM-5, 108 μmol HCOOH, and 10 mL DI H₂O with 5 bar CO, and mixture of 28 mg 0.10 wt%Rh/ZSM-5, 108 μmol HCOOH, and 10 mL DI H₂O with 10 bar CO. As shown in Supplementary Fig. 7, no acetic acid was formed in these experiments.

Direct participation of CH₄ in formation of CH₃COOH. The influence of CH₄ pressure on the catalytic performance was explored at 150 °C under a mixture of 10 bar CO and 8 bar O₂ and different pressure of CH₄ (10, 20, 30, 40, and 50 bar) for 2 h (Fig. 3c). The progressive increase of yield of acetic acid along the increase of CH₄ pressure shows that CH₄ directly participates into the formation of acetic acid (Fig. 3c), which excluded a pathway in which CH₄ couples with formic acid to form acetic acid. If acetic acid were formed from a coupling of formic acid with CH₄, the amount of formic acid should have decreased along the increase of pressure of CH₄ since more formic acid should have been consumed along with the increased amount of CH₄.

To elucidate the source of carbon atoms at the molecular level, ¹³CH₄ isotope experiments were performed. 0.7 bar ¹³CH₄ (Aldrich, 99 at%) was mixed with 13.3 bar of CH₄, 7.0 bar CO, and 8.0 bar O₂ for isotope experiment on 28 mg of 0.10 wt%Rh/ZSM-5 at 170 °C for 10 h (Fig. 4c). A control experiment using 14

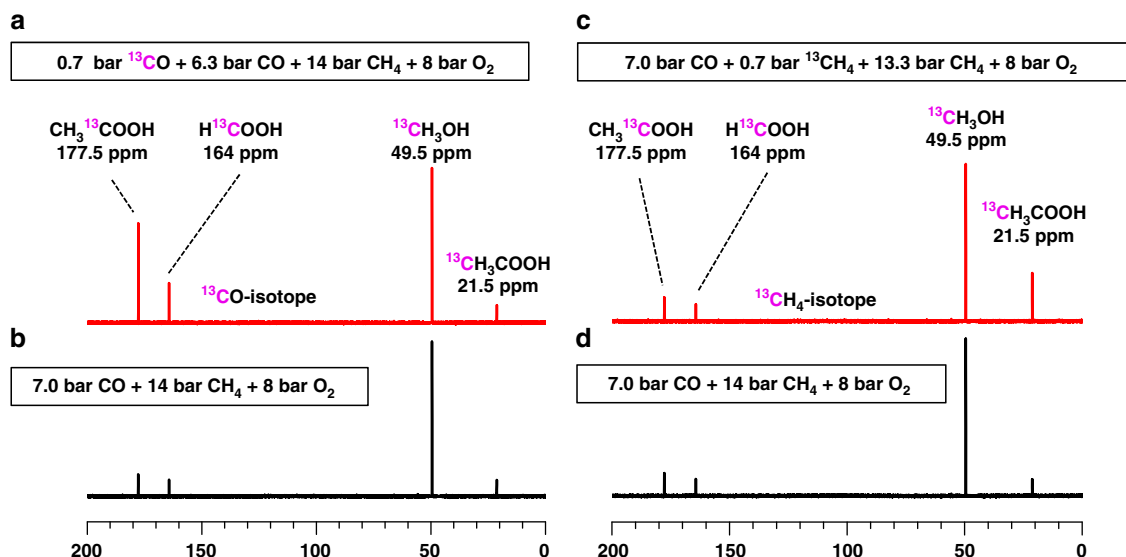


Fig. 4 ^{13}C NMR studies of reaction using ^{13}CO or $^{13}\text{CH}_4$. ^{13}C NMR spectra of products of acetic acid, formic acid, and methanol on 28 mg 0.10 wt%Rh/ZSM-5 at 170 °C for 10 h in gas of **a** mixture of 0.7 bar ^{13}CO , 6.3 bar CO, 14 bar CH_4 , and 8 bar O_2 , **b** mixture of 7 bar CO, 14 bar CH_4 , and 8 bar O_2 , **c** mixture of 7 bar CO, 0.7 bar $^{13}\text{CH}_4$, 13.3 bar CH_4 , and 8 bar O_2 , and **d** mixture of 7 bar CO, 14 bar CH_4 , and 8 bar O_2 . **a** and **b** are isotope experiments; **c** and **d** are their corresponding contrast experiments

bar unlabeled CH_4 was performed under the exactly same catalytic condition (Fig. 4d). $^{13}\text{CH}_3\text{COOH}$ were formed in the two experiments. However, their ratio of $^{13}\text{CH}_3\text{COOH}$ to reference ($^{13}\text{CH}_3\text{OH}$) when $^{13}\text{CH}_4$ was used (Fig. 4c), is much larger than that when unlabeled CH_4 was used (Fig. 4d). This difference shows that the carbon atom of CH_3 of acetic acid comes from CH_4 instead of CO. If C atoms of $\text{C}=\text{O}$ of CH_3COOH could come from CH_4 , the ratio of $\text{CH}_3^{13}\text{COOH}$ to reference ($^{13}\text{CH}_3\text{OH}$) in Fig. 4c would be much larger than the ratio in Fig. 4d since the experiment of Fig. 4d contains significant amount of $^{13}\text{CH}_4$. In fact, in both experiments (Fig. 4c, d), we did observe small amount of $\text{CH}_3^{13}\text{COOH}$ but there is no difference between their ratios to reference ($^{13}\text{CH}_3\text{OH}$) in the experiments of both Fig. 4c, d. Here, the formation of $\text{CH}_3^{13}\text{COOH}$ is due to the natural abundance of ^{13}CO in unlabeled CO. Thus, CO does not contribute to the formation of CH_3 of CH_3COOH .

Direct coupling of reactants for formation of acetic acid. It is noted that the amounts of the observed methanol in any of our studies of this work are always much lower than acetic acid and formic acid. One potential argument for the low yield of methanol could be that methanol has been formed but it could have acted as an intermediate compound in the formation of acetic acid; in other words, formic acid could have been consumed through coupling with CO to form acetic acid. Depending on whether CH_3OH could act as an intermediate product in the formation of acetic acid or not, two categories of potential pathways α and β were proposed in Fig. 5a. In potential pathway α , CH_4 couples with CO to directly form acetic acid; methanol is not an intermediate product of this type of reaction pathway. In potential pathway β , however, CH_3OH is an intermediate product and then be consumed in the formation of acetic acid; CH_4 is first oxidized to CH_3OH (the first step) and then CH_3OH couples with CO to form acetic acid (the second step); the second step of the potential pathway β is called carbonylation of methanol by CO; it is in fact the Monsanto process^{29–31}. In order to identify whether CH_3OH carbonylation (pathway β) could be a pathway for the production of acetic acid on our catalyst $\text{Rh}_1\text{O}_5@ZSM-5$, carefully designed isotope experiments described in Supplementary Methods were performed.

These isotope experiments show that acetic acid cannot be formed from carbonylation of methanol by CO on our catalyst. In one isotope-labeled experiment, 1.0 mmol isotope-labeled $^{13}\text{CH}_3\text{OH}$ (99 atom% ^{13}C , Aldrich) was added to 10 mL deionized H_2O before introduction of 10 bar CH_4 , 5 bar CO, and 4 bar O_2 to the Parr reactor. If CH_3OH could not be an intermediate for formation of acetic acid, the added $^{13}\text{CH}_3\text{OH}$ would not participate into the formation of isotope-labeled acetic acid, $^{13}\text{CH}_3\text{COOH}$. Thus, no $^{13}\text{CH}_3\text{COOH}$ could be observed if carbonylation of methanol by CO would not be involved (possibility 1 in Fig. 5b). The NMR spectrum of the solution of products formed in the reactor having $^{12}\text{CH}_4$, ^{12}CO , and O_2 ($^{13}\text{CH}_3\text{OH}$ was not added) after reaction of 2 h was presented in Fig. 5c. Figure 5d is the NMR spectrum of the products formed after the catalysis for 1 h under a condition of mixture of $^{13}\text{CH}_3\text{OH}$, $^{12}\text{CH}_4$, ^{12}CO , and O_2 at 150 °C. The observed peaks A, B, C, D, and E in Fig. 5d were assigned to CH_3COOH , CH_3OH , HCOOH , $^{13}\text{CH}_3\text{OH}$, and H^{13}COOH , respectively. As neither peak of H atoms of $^{13}\text{CH}_3$ of $^{13}\text{CH}_3\text{COOH}$ in ^1H spectrum nor peak of ^{13}C atoms of $\text{CH}_3^{13}\text{COOH}$ in ^{13}C spectrum was observed in the NMR, pathway β is not a pathway for formation of acetic acid. Thus, these isotope studies showed that acetic acid is not formed from carbonylation of methanol by CO. Additionally, H^{13}COOH was observed clearly in Fig. 5d, suggesting that $^{13}\text{CH}_3\text{OH}$ can be oxidized to H^{13}COOH under the current catalytic condition.

We also performed the dry reforming of CH_4 by CO_2 by introducing 30 bar CH_4 and 30 bar CO_2 to the reactor containing 10 mL H_2O and well dispersed 28 mg of 0.10 wt%Rh/ZSM-5. The reactor was heated to 150 °C and remained at 150 °C for 5 h and then cooled to 10 °C in ice water. As shown in Supplementary Fig. 6d, NMR test shows none of these products (acetic acid, formic acid, and methanol) was formed.

Ready separation of products from hydrophobic solvent. The above chemical transformation was performed in aqueous solution. As the products of this chemical transformation, acetic acid, formic acid, and methanol are hydrophilic, it is not readily to separate these hydrophilic products from water. To make these hydrophilic products automatically separate from solvent after synthesis, a hydrophobic solvent, *n*-dodecane was used. As shown

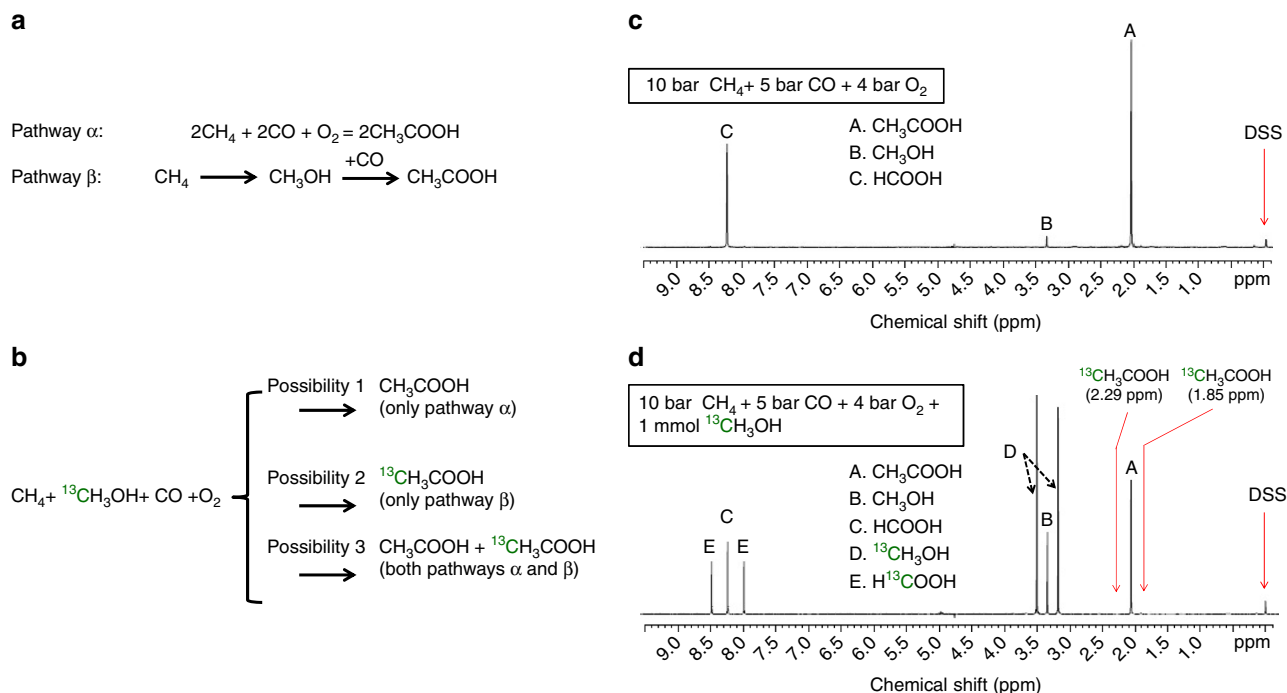


Fig. 5 Isotope studies for elucidating whether acetic acid could be formed through coupling methanol with CO. **a** Two potential pathways α and β for production of acetic acid; in pathway α , CH_3OH is not an intermediate compound for formation of CH_3COOH ; in pathway β , CH_3OH is an intermediate compound for formation of CH_3COOH . **b** Potential catalytic products formed from 0.10 wt%Rh/ZSM-5 in the mixture of $^{13}\text{CH}_3\text{OH}$ and H_2O in solution under mixture of CH_4 , CO , and O_2 if the transformation of CH_4 , CO , and O_2 follows pathway α , β , or both α and β . **c** NMR spectra of the products formed from 28 mg of 0.10 wt%Rh/ZSM-5 after reaction in 10 bar CH_4 , 5 bar CO , and 4 bar O_2 at 150 °C for 1 h; there was no any isotope-labeled methanol, $^{13}\text{CH}_3\text{OH}$ added to the reactor before this catalysis test. **d** NMR spectra of the products formed from 28 mg of 0.10 wt%Rh/ZSM-5 after reaction in 10 bar CH_4 , 5 bar CO , and 4 bar O_2 at 150 °C for 1 h; notably, 1.0 mmol $^{13}\text{CH}_3\text{OH}$ was added to H_2O before this catalysis test

in Supplementary Fig. 8 28 mg 0.10 wt%Rh/ZSM-5 in 10 mL *n*-dodecane in the mixture of 30 bar CH_4 , 10 bar CO , and 5 bar O_2 is definitely active for the formation of acetic acid. The significant advantage of using the hydrophobic solvent is that the hydrophilic products of this reaction including acetic acid, methanol, and formic acid can be readily separated from the hydrophobic solvent, without or with a low energy cost.

Feature of this mild oxidation of methane in solution. CH_4 and CO can be oxidized with different oxidants including O_2 , concentrated H_2SO_4 , or a superacid^{32–34} by using homogeneous catalyst³², in which acetic acid and other products (formic acid and methanol) were formed. One control experiment using Rh (NO_3)₃ was done (entry 3 in Table 1); the turn-over-rate (TOR) of the homogenous catalyst, Rh(NO_3)₃ without a promoter is only 6.3×10^{-6} molecules per rhodium cation per second at 150 °C. Here, the Rh_1O_5 @ZSM-5 catalyzes the oxidation of CH_4 and CO with a low-cost oxidant, molecular oxygen or even air at 150 °C at a solid–liquid–gas interface. TOR of the catalytic sites Rh_1O_5 anchored in microporous silicate reaches 0.070 CH_3COOH molecules on per Rh_1O_5 site per second in mixture of 50 bar CH_4 , 10 bar CO , and 8 bar O_2 (entry 2 of Table 1). These TORs for production of acetic acid on singly dispersed site Rh_1O_5 are much higher than those reported homogenous catalysts^{32,33} by >1000 times. As shown in Fig. 2, 840 μmol of acetic acid, 352 μmol of formic acid, and 82 μmol of methanol were produced from 28 mg 0.10 wt%Rh/ZSM-5 at 150 °C for 12 h under a catalytic condition of 50 bar CH_4 , 10 bar CO and 8 bar O_2 , which correspond to conversion of 10.2% of CH_4 under this condition. Selectivity for production of acetic acid among all organic products reaches about 70% under this condition. Other than the highest catalytic

efficiency on Rh_1O_5 @ZSM-5, a significant advantage of our catalytic process is the ready separation of liquid products from the solid catalyst and solvent.

It is found that a shorter reaction time gives a higher selectivity for formation of formic acid and a longer reaction time lead to a higher selectivity for formation of acetic acid. As shown in Supplementary Fig. 9 both formic acid and acetic acid are the main products when reaction time is shorter than 3 h. When the reaction time is 3 h or longer, acetic acid is the main product. The evolution of the yields of formic acid and acetic acid as a function of time implies that the relative low temperature of catalyst in the heating from 25 to 150 °C is favorable for the formation of formic acid. More discussion on time-dependent selectivity for formation of formic acid and acetic acid can be found from Supplementary Discussion.

Understanding reaction mechanism at molecular level. Based on the coordination environment of Rh_1 atoms suggested by EXAFS studies, we used a structural model whose Rh atom bonds with three oxygen atoms of the substrate wall and two oxygen atoms of one oxygen molecule in our computational studies. Our DFT calculations suggest that the Rh atom prefers a ten-membered-ring channel, which has smaller repulsion, instead of a six-membered ring channel of ZSM-5. Based on the experimental preparation method, we expect that the Rh_1 cations replace the Bronsted sites and thus bind to the Al atoms. As shown in Fig. 6a this Rh_1 atom binds to three oxygen atoms of the Si–O framework and two oxygen atoms of reactant, making Rh_1 exhibit positive to 0.927 |e|.

Isotope experiments suggest two necessary steps: activation of C–H bond of CH_4 to form CH_3 and insertion of CO to form

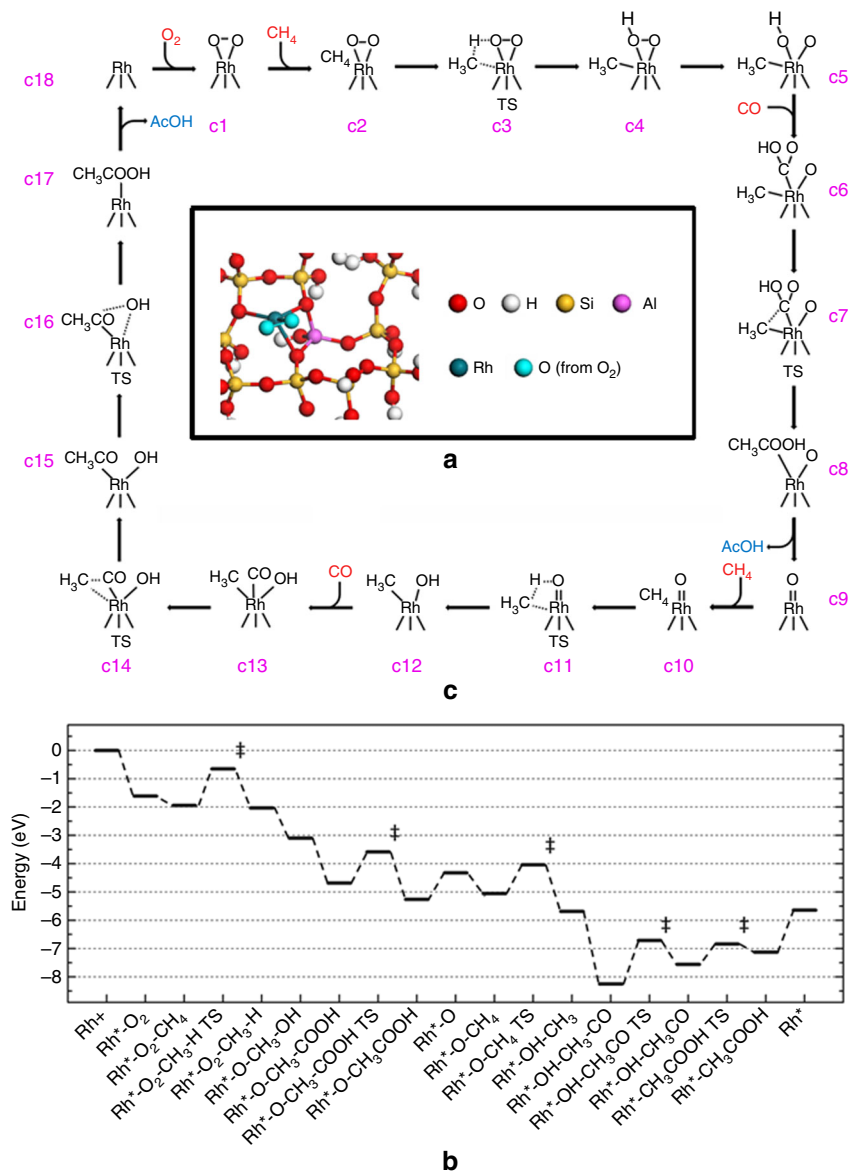


Fig. 6 Computational studies of reaction pathway. Minimum-energy paths and reaction schematic for formation of acetic acid from CH₄, CO, and O₂ on Rh₁O₅/ZSM-5. The formation of acetic acid is illustrated in a catalytic cycle starting with the singly dispersed Rh₁O₅ site. The balanced reaction cycle consumes one O₂, two CH₄, and two CO to make two CH₃COOH molecules (2CH₄+2CO+O₂=2CH₃COOH). **a** The optimized catalytic sites, Rh₁O₅ anchored on Brønsted site in microspore of ZSM-5. **b** Energy profile for pathway of transforming CH₄, CO, and O₂ to CH₃COOH. **c** Intermediates and transition states for a complete catalytic cycle, starting with Rh₁O₅ (c1). Transition states are highlighted with the double dagger symbols

acetic acid. Based on these experimental findings, reaction pathway on the Rh₁O₅ with lowest energy was simulated and transition states were located (Fig. 6). The energy profile and catalytic cycle are illustrated in Fig. 6b, c, respectively. The specific energies are listed in Supplementary Table 3. We found that the Rh₁O₅ active site (Fig. 6a) participates in the reaction by first activating C–H bond of methane (c2 and c3) with an activation barrier of 1.29 eV. It forms a methyl and hydroxyl adsorbed on the Rh atom (c4). Then, a CO molecule can insert to the Rh–O bond of Rh–O–H, forming a COOH adsorbed on Rh (c6). Then COOH can couple with the adsorbed methyl with a barrier of 1.11 eV (c7), forming a weakly adsorbed acetic acid (c8). Subsequent desorption yields the first CH₃COOH molecule. The remaining Rh–O oxo group (c9) activates C–H bond of the second CH₄ molecule to form a methyl and a hydroxyl group adsorbed on the Rh atom (c12). Following, or concurrently to this step, the second CO molecule binds to the unsaturated Rh

site (c13). Then, the adsorbed CO inserts into the methyl–Rh bond with a barrier of 1.54 eV (c14), forming an acetyl group (c15). Finally, the hydroxyl group couples with carbon atom of C=O of the acetyl group to form the second acetic acid with a barrier of 0.72 eV (c17). Desorption of the second acetic acid molecule recovers the Rh site (c18), which then bonds with a molecular O₂, forming a Rh₁O₅ site (c1) ready for next catalytic cycle.

Our experimental studies show that high pressure of CO (Fig. 3b) in fact decreased the activity for producing acetic acid and finally poisoned the active sites. Computational study explored the observed influence of CO pressure on the catalytic activity. It suggests that saturated coordination of Rh with CO molecules under CO gas at a high pressure can poison a Rh₁ site and thus prevent it from forming acetic acid. In addition, the DFT calculations show the activation energy for C–H of CH₄ is largely increased if the Rh₁ pre-adsorbed two CO molecules at high-

pressure of CO (Supplementary Fig. 10b). More information can be found in Supplementary Discussion.

In summary, the heterogeneous catalyst, 0.10 wt%Rh/ZSM-5 consisting of singly dispersed Rh_1O_5 sites anchored in the micropores of microporous aluminate silicate was prepared. The anchored Rh_1O_5 sites exhibit unprecedented catalytic activity in synthesis of acetic acid higher than free Rh^{3+} in aqueous solution by >1000 times under mild conditions. This heterogeneous catalytic process opens a new route to synthesize acetic acid through direct utilization of methane under a mild condition at 150 °C or lower by using a low-cost oxidant, O_2 or air instead of current industrial process of synthesizing acetic acid through carbonylation of methanol.

Methods

Preparation and characterization of catalyst. Two steps were involved in the preparation of a Rh/ZSM-5 catalyst. The first step is the preparation of H-ZSM-5 by calcining zeolite $\text{NH}_4\text{-ZSM-5}$ with a $\text{SiO}_2/\text{Al}_2\text{O}_3$ ratio of 23 (Alfa Aesar) in air at 400 °C for 12 h. Four Rh/ZSM-5 catalysts with different Rh concentrations (0.01 wt %, 0.05 wt %, 0.10 wt %, 0.50 wt %) were synthesized through a method integrating vacuum pumping and IWI of aqueous solution containing certain amount of rhodium(III) nitrate hydrate (~36% Rh basis, Sigma-Aldrich) at room temperature. Typically, 500 mg of H-ZSM-5 was placed in a 50 mL three-port flask. The three ports were sealed with three corks. One port was connected to a vacuum pump. Before injection of $\text{Rh}(\text{NO}_3)_3$ solution, air in the flask containing 100 mg H-ZSM-5 was purged for 3–5 h by a vacuum pump when the H-ZSM-5 powder was being stirred. The size of stirring bar is 5 mm for maximizing the amount of H-ZSM-5 to be stirred. Then, 0.30 mL of 1.0 mg/mL $\text{Rh}(\text{NO}_3)_3$ aqueous solution was added to the H-ZSM-5, which had been pumped for 3–5 h. The injection needle quickly reached the powder to avoid the dispersion of solution to the wall of flask since the environment of flask is in vacuum. In addition, the tip of needle was buried in the middle of H-ZSM-5 powder during injection, minimizing diffusion of solution to the wall of flask. During the injection, the H-ZSM-5 should be continuously stirred.

After the introduction of Rh^{3+} , the samples were further dried in an oven at 80 °C for 3 h and calcined in air at 550 °C for 3 h. Supplementary Fig. 1 schematically shows the evolution of the structure of the anchored Rh atoms in ZSM-5 of 0.10 wt%Rh/ZSM-5. Actual Rh contents were determined by inductively coupled plasma atomic emission spectrometry (ICP-AES). TEM (FEI, Titan 80–300) was used to characterize the morphology of the catalyst. EXAFS of Rh K-edge was taken at SPring-8. For EXAFS studies, the used catalyst of 0.10 wt%Rh/ZSM-5 was measured when the catalyst was kept at 150 °C in the flow of pure He. The adsorption fine structure spectra of Rh K-edge were fitted using IFEFFIT package and FEFF6 theory. Reference samples including Rh metal foil and Rh_2O_3 nanoparticles supported on Al_2O_3 were studied with EXAFS. Their r-space spectra of these reference samples were fitted with the same software. XPS was performed using a PHI5000 VersaProbe Spectrometer with monochromated Al K α as X-ray source.

Catalytic reactions. Transformation of methane to acetic acid on 0.10 wt%Rh/ZSM-5 was performed in a Parr high-pressure reactor (Series 4790, Parr) containing a Teflon liner vessel (Supplementary Fig. 3b). 28 milligram 0.10 wt%Rh/ZSM-5 was added to 10 mL H_2O in the reactor. After evacuating the air left in reactor by flowing CH_4 (99.9%, Matheson) and purging for five times, the system was pressurized with reactant gases in a sequence of CH_4 , CO (99.9%, Matheson) and O_2 (99.9%, Matheson) to their desired pressures. The high-pressure reactor was completely sealed and then heated to the desired reaction temperature (typically 150 °C) by placing it in an oil bath. The temperature controller of the heating plate (VWR International) was used to measure the temperature of solution in the Parr reactor through the thermocouple placed in solution of Parr reactor and to control the temperature through outputting tunable power to the heating plate. Once the desired catalysis temperature was reached, the solution was vigorously stirred at 1200 rpm and was maintained at the reaction temperature for certain amount of time. After completion of the reaction, the vessel was cooled in an ice bath to a temperature below 10 °C to minimize the loss of volatile products. The solution with liquid products was filtered from the catalyst powder. The clean liquid containing acetic acid, formic acid, and methanol was analyzed by $^1\text{H-NMR}$ or $^{13}\text{C-NMR}$. The concentration of Rh in the filtered powder was examined with ICP-AES as described in Supplementary Methods. Supplementary Fig. 11 is the standard curve of ICP-AES studies of Rh concentrations.

Measurements of products with NMR and GC. $^1\text{H-NMR}$ spectra were collected at room temperature on a Bruker AVANCE III HD 400 spectrometer at University of Notre Dame and University of Kansas. The measurements were calibrated by using 3-(trimethylsilyl)-1-propanesulfonic acid sodium salt (DSS) residual signal at $\delta = 0.0$ ppm. Supplementary Fig. 4 is a typically NMR spectrum of products formed from CH_4 transformation. Obviously, the peak of DSS can be identified.

Typically, 0.7 mL collected filtrate and 0.1 mL of D_2O (with 0.02 wt% DSS) were mixed in an NMR tube for analysis. The identified oxygenated products were acetic acid ($\delta = 2.08$ ppm), formic acid ($\delta = 8.24$ ppm) and methanol ($\delta = 3.34$ ppm). A solvent suppression program was applied in order to minimize the signal originating from H_2O , similar to our previous studies¹¹. To quantify the products, standard curves were built using the same method as that of our previous report¹¹. To establish a standard curve of a specific product such as acetic acid, a series of standard solutions with different concentrations of acetic acid were prepared. For instance, to establish a standard curve acetic acid, a series of standard solutions with different concentrations of acetic acid were prepared. NMR spectra of these standard solutions were collected with the exactly same parameters of NMR measurements. The ratio of the area of peak of acetic acid ($\delta = 2.08$ ppm) to area of DSS of the same solution were calculated. These ratios of solutions with different concentrations of acetic acid were plotted as a function of the concentrations of acetic acid. This graph is a standard curve of acetic acid (Supplementary Fig. 5a), formic acid (Supplementary Fig. 5b), and methanol (Supplementary Fig. 5c). Concentration of a product (such as acetic acid) in a solution after catalysis in Parr reactor was determined by locating the ratio of the peak area of the product to the area of DSS on the y-axis of the standard curve (such as Supplementary Fig. 5a) and then finding the corresponding value on x-axis, which is the amount of the product of the solution after a catalysis in the unit of μmol . Gases in the head of Parr reactor after catalysis were analyzed with GC. Supplementary Table 4 presents the amounts of all reactants before catalysis and all products and left reactants after the catalysis; this catalysis was performed on 28 mg 0.10 wt%Rh/ZSM-5 dispersed in 10 mL deionized H_2O under 50 bar CH_4 , 10 bar CO, and 8 bar O_2 for 3 h. Bruker Topspin 3.5 software was used to acquire, process, and visualize the data.

Data availability. All data are available from the authors upon reasonable request

Received: 17 September 2016 Accepted: 19 January 2018

Published online: 26 March 2018

References

- Mattos, L. V., Jacobs, G., Davis, B. H. & Noronha, F. B. Production of hydrogen from ethanol: Review of reaction mechanism and catalyst deactivation. *Chem. Rev.* **112**, 4094–4123 (2012).
- Liu, Y. et al. Efficient conversion of methane to aromatics by coupling methylation reaction. *ACS Catal.* **6**, 5366–5370 (2016).
- Ali, A., Alvarez, W., Loughran, C. J. & Resasco, D. E. State of Pd on H-ZSM-5 and other acidic supports during the selective reduction of NO by CH_4 studied by EXAFS/XANES. *Appl. Catal. B: Environ.* **14**, 13–22 (1997).
- Ali, A., Chin, Y. H. & Resasco, D. E. Redispersion of Pd on acidic supports and loss of methane combustion activity during the selective reduction of NO by CH_4 . *Catal. Lett.* **56**, 111–117 (1998).
- Hammond, C. et al. Direct catalytic conversion of methane to methanol in an aqueous medium by using copper-promoted Fe-ZSM-5. *Angew. Chem. Int. Ed.* **51**, 5129–5133 (2012).
- Yoshizawa, K., Shiota, Y., Yumura, T. & Yamabe, T. Direct methane-methanol and benzene-phenol conversions on Fe-ZSM-5 zeolite: Theoretical predictions on the reaction pathways and energetics. *J. Phys. Chem. B.* **104**, 734–740 (2000).
- Kuroda, Y. et al. On the possibility of AgZSM-5 zeolite being a partial oxidation catalyst for methane. *J. Colloid Interface Sci.* **333**, 294–299 (2009).
- Mahyuddin, M. H., Staykov, A., Shiota, Y. & Yoshizawa, K. Direct conversion of methane to methanol by metal-exchanged ZSM-5 zeolite (Metal = Fe, Co, Ni, Cu). *ACS Catal.* **6**, 8321–8331 (2016).
- Gold, F. et al. Computationally exploring confinement effects in the methane-to-methanol conversion over iron-oxo centers in zeolites. *ACS Catal.* **6**, 8404–8409 (2016).
- Behrens, M. et al. The active site of methanol synthesis over Cu/ZnO/Al₂O₃ industrial catalysts. *Science* **336**, 893–897 (2012).
- Huang, W. X. et al. Low-temperature transformation of methane to methanol on Pd₁₀A single sites anchored on the internal surface of microporous silicate. *Angew. Chem. Int. Ed.* **55**, 13441–13445 (2016).
- Coperet, C. et al. Surface organometallic and coordination chemistry toward single-site heterogeneous catalysts: strategies, methods, structures, and activities. *Chem. Rev.* **116**, 323–421 (2016).
- Pelletier, J. D. A. & Basset, J. M. Catalysis by design: Well-defined single-site heterogeneous catalysts. *Acc. Chem. Res.* **49**, 664–677 (2016).
- Serna, P. & Gates, B. C. Molecular metal catalysts on supports: Organometallic chemistry meets surface science. *Acc. Chem. Res.* **47**, 2612–2620 (2014).
- Yang, X. F. et al. Single-atom catalysts: a new frontier in heterogeneous catalysis. *Acc. Chem. Res.* **46**, 1740–1748 (2013).
- Zhang, S. R. et al. Catalysis on singly dispersed bimetallic sites. *Nat. Commun.* **6**, 7938 (2015).

17. Qiao, B. T. et al. Single-atom catalysis of CO oxidation using Pt-1/FeOx. *Nat. Chem.* **3**, 634–641 (2011).
18. Tao, F. et al. Reaction-driven restructuring of Rh-Pd and Pt-Pd core-shell nanoparticles. *Science* **322**, 932–934 (2008).
19. Mulukutla, R. S., Asakura, K., Namba, S. & Iwasawa, Y. Nanosized rhodium oxide particles in the MCM-41 mesoporous molecular sieve. *Chem. Comm.* **0**, 1425–1426 (1998).
20. Mulukutla, R. S., Shido, T., Asakura, K., Kogure, T. & Iwasawa, Y. Characterization of rhodium oxide nanoparticles in MCM-41 and their catalytic performances for NO-CO reactions in excess O₂. *Appl. Catal. A: Gen.* **228**, 305–314 (2002).
21. Dent, A. J. et al. Rhodium dispersion during NO/CO conversions. *Angew. Chem. Int. Ed.* **46**, 5356–5358 (2007).
22. Martinez-Macias, C., Serna, P. & Gates, B. C. Isostructural zeolite-supported rhodium and iridium complexes: Tuning catalytic activity and selectivity by ligand modification. *ACS Catal.* **5**, 5647–5656 (2015).
23. Serna, P. & Gates, B. C. Zeolite-supported rhodium complexes and clusters: Switching catalytic selectivity by controlling structures of essentially molecular species. *J. Am. Chem. Soc.* **133**, 4714–4717 (2011).
24. Liang, A. J. et al. A site-isolated rhodium-diethylene complex supported on highly dealuminated Y zeolite: Synthesis and characterization. *J. Phys. Chem. B.* **109**, 24236–24243 (2005).
25. Yang, D., Xu, P. H., Browning, N. D. & Gates, B. C. Tracking Rh atoms in zeolite HY: First steps of metal cluster formation and influence of metal nuclearity on catalysis of ethylene hydrogenation and ethylene dimerization. *J. Phys. Chem. Lett.* **7**, 2537–2543 (2016).
26. Wu, J. F. et al. Mechanistic insight into the formation of acetic acid from the direct conversion of methane and carbon dioxide on zinc-modified H-ZSM-5 zeolite. *J. Am. Chem. Soc.* **135**, 13567–13573 (2013).
27. Yu, Z. W. et al. Bronsted/Lewis acid synergy in H-ZSM-5 and H-MOR zeolites studied by H-1 and Al-27 DQ-MAS solid-state NMR spectroscopy. *J. Phys. Chem. C.* **115**, 22320–22327 (2011).
28. Shan, J. J. et al. Conversion of methane to methanol with a Bent Mono(mu-oxo)nickel anchored on the internal surfaces of micropores. *Langmuir* **30**, 8558–8569 (2014).
29. Budiman, A. W. et al. Review of acetic acid synthesis from various feedstocks through different catalytic processes. *Catal. Surv. Asia* **20**, 173–193 (2016).
30. Kinnunen, T. & Laasonen, K. The oxidative addition and migratory 1,1-insertion in the Monsanto and Cativa processes. A density functional study of the catalytic carbonylation of methanol. *J. Mol. Struct. Theochem.* **542**, 273–288 (2001).
31. Maitlis, P. M., Haynes, A., Sunley, G. J. & Howard, M. J. Methanol carbonylation revisited: Thirty years on. *J. Chem. Soc., Dalton Trans.* **0**, 2187–2196 (1996).
32. Lin, M. & Sen, A. Direct catalytic conversion of methane to acetic acid in an aqueous-medium. *Nature* **368**, 613–615 (1994).
33. Periana, R. A., Mironov, O., Taube, D., Bhalla, G. & Jones, C. J. Catalytic, oxidative condensation of CH₄ to CH₃COOH in one step via CH activation. *Science* **301**, 814–818 (2003).
34. Zerella, M., Mukhopadhyay, S. & Bell, A. T. Direct oxidation of methane to acetic acid catalyzed by Pd²⁺ and Cu²⁺ in the presence of molecular oxygen. *Chem. Comm.* **0**, 1948–1949 (2004).

Acknowledgements

This work was solely supported by the U.S. Department of Energy, Office of Science, Office of Basic Energy Sciences, Chemical Sciences, Geosciences, and Biosciences Division under Award Number DE-SC0014561 of Catalysis Science Program. Y.L. and F.T. appreciated J. Douglas of NMR lab of KU for valuable discussion in solid-state NMR data measurements. J. Shan learnt sample preparation and catalysis studies of this work in the years 2013 and 2014 when being trained for studies of catalysis in liquid. A.I.F. is partially supported by the U.S. DOE Grant No. DE-FG02-03ER15476.

Author contributions

Y.T., Y. L. and V.F. equally contributed to this work. F.T. developed the concept, designed these experiments, analyzed experimental data, and wrote the paper. W.H, S.Z., Y.T., Y.L., L.N. and X.Z. performed catalyst preparation and catalytic measurements and analysis of data. Y.F. and D.J. developed computational studies. Y. T., Y.L., T.S., and A.I.F. collected and analyzed XAS data. All authors discussed the results and commented on the manuscript.

Additional information

Supplementary Information accompanies this paper at <https://doi.org/10.1038/s41467-018-03235-7>.

Competing interests: The authors declare no competing financial interests.

Reprints and permission information is available online at <http://npg.nature.com/reprintsandpermissions/>

Publisher's note: Springer Nature remains neutral with regard to jurisdictional claims in published maps and institutional affiliations.



Open Access This article is licensed under a Creative Commons Attribution 4.0 International License, which permits use, sharing, adaptation, distribution and reproduction in any medium or format, as long as you give appropriate credit to the original author(s) and the source, provide a link to the Creative Commons license, and indicate if changes were made. The images or other third party material in this article are included in the article's Creative Commons license, unless indicated otherwise in a credit line to the material. If material is not included in the article's Creative Commons license and your intended use is not permitted by statutory regulation or exceeds the permitted use, you will need to obtain permission directly from the copyright holder. To view a copy of this license, visit <http://creativecommons.org/licenses/by/4.0/>.

© The Author(s) 2018